THE JOURNAL OF PHYSICAL CHEMISTRY C
A JOURNAL OF THE AMERICAN CHEMICAL SOCIETY

pubs.acs.org/JPCC

Article

Valence Band Structure Degeneracy Enhanced Thermoelectric Performance in β-Cu_2Se

Xiaomeng Cai,[§] Huirong Jing,[§] Hexige Wuliji, and Hong Zhu*

Cite This: https://doi.org/10.1021/acs.jpcc.2c08797

Read Online

ACCESS | Metrics & More | Article Recommendations | Supporting Information

ABSTRACT: Cu_2Se is known to be a promising p-type thermoelectric material resulting from its extremely low thermal conductivity. On the other hand, compared to other high-performance thermoelectric materials like PbTe, the valence band degeneracy of Cu_2Se is 4 times lower, which is believed to be unfavorable to the power factor. In this work, band structure engineering has been applied to increase the band degeneracy of Cu_2Se through effective doping. Based on the careful analysis of bonding characters and atomic energy levels in the Cu_2Se compound, some defects (the Fe or Mn substitutional defects, Fe_{Cu} or Mn_{Cu}, and the copper vacancy, V_{Cu}) are predicted to be able to converge two valence band maxima in Cu_2Se. The electrical transport properties of Cu_2Se with different defects (V_{Cu}/Fe_{Cu}/Mn_{Cu}) have been studied based on first-principles electronic structure calculations. A Boltzmann transport study demonstrates that the weakened p−d orbital interaction may enhance the electrical transport properties in Cu_2Se.

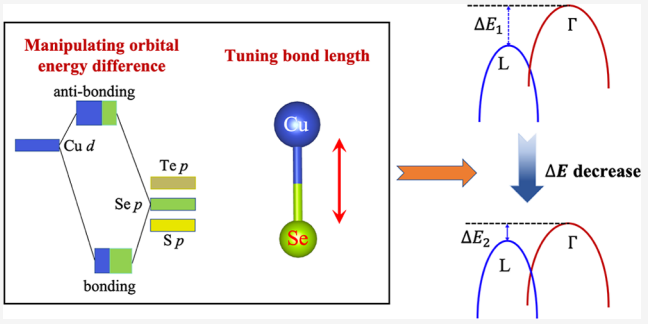

INTRODUCTION

Thermoelectric materials, capable of converting thermal into electric energy and vice versa, have great potential to be used for waste heat recovery and power generation. The performance of thermoelectric materials is usually described by the dimensionless figure of merit (zT), defined as $S^2\sigma T/(\kappa_e + \kappa_L)$, where S, σ, T, κ_e, and κ_L are the Seebeck coefficient, electrical conductivity, absolute temperature, electrical thermal conductivity, and lattice thermal conductivity, respectively. The continuous increase of zT over the past decades has been achieved through successful reduction of the thermal conductivity, that is, via solid-solution alloying[1−3] and nanostructuring,[4] and the enhancement of the power factor (PF = $S^2\sigma$), that is, via band structure engineering.[5−8]

The power factor is strongly related to $N_V\mu(m_b^*/m_e)^{3/2}$, where N_V is the valley degeneracy, μ is the carrier mobility, m_b^* is the density of states (DOS) effective mass for each valley, and m_e is the free electron mass.[9] Converging individual carrier pockets to increase N_V without deteriorating μ is a straightforward scheme for improving the thermoelectric performance. As reported in previous works, doping is an effective approach to modify the band structure to realize the band convergence.[8,10−12] For example, enhanced zT was verified in Mg-,[13] Mn-,[14] Cd-,[15] and Tl-doped[11] PbTe resulting from the increased number of valence valley. Similarly, a comparable zT of 1.3 around 700 K was realized in Sn-doped Mg_2Si owing to the converged conduction bands.[16] Obviously, band convergence is an effective method to improve the thermoelectric performance.

Cu_2Se (namely, β-Cu_2Se, $Fm\bar{3}m$ space group) is a promising thermoelectric material for high-temperature application, with extremely low thermal conductivity originated from the liquid-like motion of the Cu ions.[17−19] Cu_2Se is a p-type semiconductor intrinsically and shows a peak zT of 2.1 at 973 K.[20] It is discovered that the valence band maximum (VBM) of Cu_2Se is located at the Γ point with a low degeneracy of 3, and the secondary lower VBM is located at the L point with a high degeneracy of 8.[21−23] Such a feature suggests that band structure engineering is possible to be utilized to improve the thermoelectric performance of p-type Cu_2Se. The valence band edge of Cu_2Se comprises quite strong p−d hybridization, which originates from the small energy difference between the atomic orbitals of Cu-d and Se-p orbitals.[18] Therefore, tuning the p−d hybridization strength by choosing appropriate dopants provides a potentially applicable scheme to regulate the thermoelectric performance of Cu_2Se.

The optimization of the thermoelectric properties of Cu_2Se has been investigated experimentally with different dopants,

Received: December 15, 2022
Revised: February 7, 2023

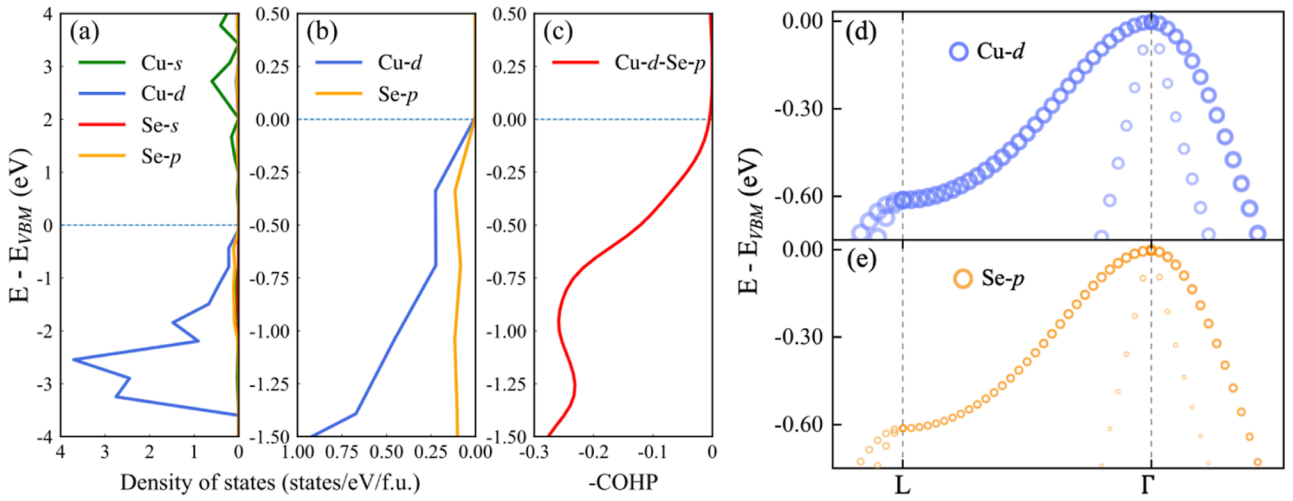

Figure 1. PDOS of the (a) Cu_2Se and (b) Cu-d and Se-p orbitals around the VBM and the (c) −COHP of Cu-d−Se-p interaction in Cu_2Se. The projected band structure with the size of the blue and orange circles at the valence band top representing the characteristic weight of (d) Cu-d and (e) Se-p orbitals, respectively.

such as Li,[24] Mg,[25] Bi,[26] Mn,[27] Fe,[27] and Ni[28] at the Cu site. Doping main group elements like Li in Cu_2Se is helpful to tune the carrier concentration, thereby increasing the electrical conductivity, but the Seebeck coefficient is decreased at the same time, and the power factor is not improved essentially. On the other hand, doping transition metals like Fe in Cu_2Se can increase the power factor, which suggests that the substitution of Cu with Fe might modify the band structure and successfully decouple the trade-off relationship between the Seebeck coefficient and the electrical conductivity.[27,29] However, there is a lack of study on the theoretical band structure analysis for transition metal-doped Cu_2Se and the effect on the thermoelectric properties to provide a deep understanding of the role of extrinsic dopants. In addition to doping foreign atoms, introducing vacancies can also play a role in band structure modification, for example, Tan et al.[30] reported that the Sn vacancies in SnTe can reduce the energy separation between the light and heavy valence bands and hence achieve a better band convergence. In addition, some recent discussions on the practical improvement of thermoelectric performance by band degeneracy make our theoretical study even more necessary. Snyder et al.[31] considered that when valley degeneracy occurs at one *k*-point, a strong deformation-potential scattering will generate, which is not conducive to thermoelectric performance improvement. In Xiong et al.[32] and Xia et al.[33] study, band degeneracy also did not achieve power factor improvement.

In this work, the electronic structure of β-Cu_2Se is investigated via first-principles calculation. Based on the atomic orbital analysis of Cu_2Se near the valence band edge, we first uncover the correlation between the band degeneracy and the atomic orbital hybridization strength. It is found that decreasing the p−d orbital interaction strength, for example, by increasing the p−d orbital energy difference or the bond length, can improve the band degeneracy. Considering the feasibility, we choose some defects which can result in a larger p−d orbital energy difference to improve the band degeneracy. Results show that transition metal (Mn, Fe) substitution and Cu vacancy introduction (V_{Cu}) in β-Cu_2Se can be used to improve the band degeneracy. The designed band structure engineering is further confirmed by the band structure calculations based on density functional theory (DFT). A Boltzmann transport study demonstrates that the Seebeck coefficients of Cu_2Se with $V_{Cu}/Fe_{Cu}/Mn_{Cu}$ defects are all higher than that of the Cu_2Se pristine compound.

METHODS

First-principles calculations were implemented in the Vienna ab initio simulation package (VASP) based on DFT.[34,35] The projector-augmented wave technique was utilized to model the interaction between electrons and ions,[36] and the Perdew−Burke−Ernzerhof (PBE) form of generalized gradient approximation was used as the exchange−correlation functional.[37] The plane wave cutoff energy was set to 500 eV in all calculations. To reasonably describe the orbital occupancies, we used a Gaussian smearing width of 0.01 eV. The electronic structures and the transport properties were calculated by using the modified Becke−Johnson (mBJ) potential,[38] and the Hubbard-*U* correction with Dudarev's approach was used. An effective Coulomb *U* ($U_{eff} = U - J$) of 4 eV[21] for Cu and other doped transition metals (Mn/Fe) was obtained. Figures S1−S3 compare the effect of different *U* values of transition elements (Cu, Fe, and Mn) on the electronic structure of the system, and it can be seen that small changes in the *U* value of Cu have some effect on the band gap of Cu_2Se, but they hardly affect the band structure near the VBM. For Mn and Fe, the band structures are almost unchanged for different *U* values. Brillouin zone sampling was performed by employing a Monkhorst−Pack *k*-mesh of 6 × 6 × 6, and the *k*-point convergence test was performed. We displayed the crystal structural and lattice parameter of β-Cu_2Se in the Supporting Information. All defective Cu_2Se results were carried out on the 2 × 2 × 2 supercell. For the calculation of the effective band structure, the supercell vectors were fixed, while the atomic positions were optimized. For other calculations, supercells were fully optimized despite very small lattice changes, and a detailed comparison can be seen in the Supporting Information. Due to the presence of unpaired electrons in Mn and Fe, spin polarization is considered in our work.

Chemical bonding analyses were carried out based on crystal orbital Hamiltonian population (COHP) using LOB-

https://doi.org/10.1021/acs.jpcc.2c08797
J. Phys. Chem. C XXXX, XXX, XXX−XXX

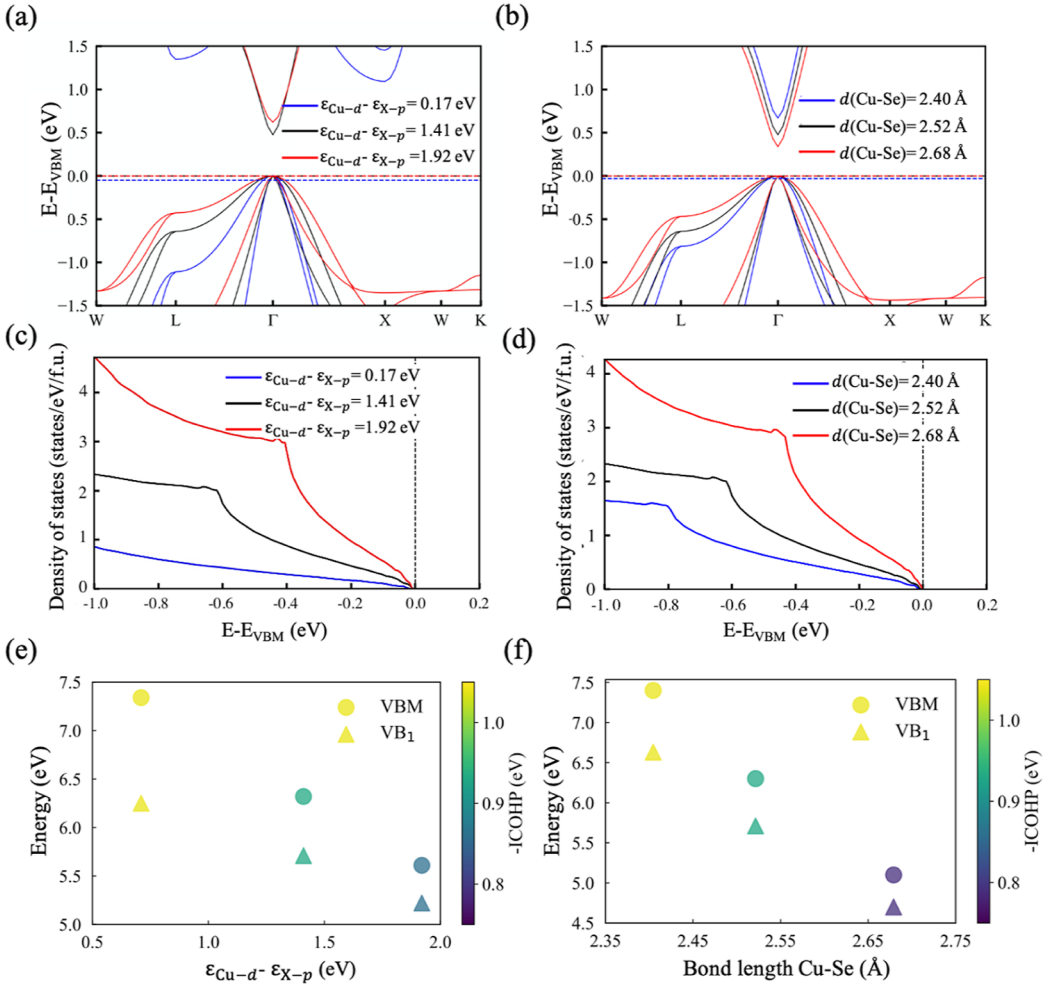

Figure 2. (a,c) Band structures and DOS of Cu_2X (X = S, Se, Te) with different orbital energies between Cu-d and X-p ($\varepsilon_{Cu\text{-}d}-\varepsilon_{X\text{-}p}$) under a fixed Cu−X bond length of 2.52 Å (b,d) and Cu_2Se with different Cu−Se bond lengths (d(Cu−Se)). The VBM has been shifted to 0 eV. Energy position of valence band maxima, VBM and VB_1, and integrated COHP (ICOHP) for (e) Cu_2X (X = S, Se, and Te) as a function of $\varepsilon_{Cu\text{-}d}-\varepsilon_{X\text{-}p}$ with a fixed d(Cu−X) of 2.52 Å and (f) Cu_2Se as a function of d(Cu−Se). The band alignment is obtained by aligning the Cu-1s core levels of different compounds. The Fermi energy corresponding to various atomic p−d orbital energy differences and various bond lengths are marked with dashed lines in (a,b).

STER.[39−41] Effective band structures were calculated by the band unfolding method using VASPKIT.[42] The electrical transport properties were calculated using the BoltzTraP package.[43] As the relaxation time (τ) is an undetermined quantity in our simulations, quantities which depend on the τ are reported by scaling them with τ (i.e., σ/τ and $S^2\sigma/\tau$).

RESULTS AND DISCUSSION

Cu_2Se is normally believed to be a semiconductor with an optical gap of 1.23 eV.[44] In our work, a comparison of the band structure with PBE, HSE, and mBJ + U functionals is displayed in Figure S8, and only mBJ + U shows a threefold degenerate valence band with non-zero gap, which is similar to pervious work.[21,22] To have a clear understanding of electronic properties of β-Cu_2Se, the atomic orbital projected DOS (PDOS) and band structure of Cu_2Se were obtained by DFT calculation and are summarized in Figure 1. The atomic orbital PDOS in Figure 1a indicates that the valence band has predominantly Cu-d and Se-p characters. It is further found from Figure 1b that the DOS of the Cu-d orbital has a similar shape to that of the Se-p orbital around the VBM, which indicates an orbital hybridization between them. From our calculated atomic orbital energy, Cu 3d orbital energy is slightly higher than that of the Se 4p orbital. Previous work found that Cu-d and Se-p characters in the VBM can be considered as the p−d anti-bonding state. This is confirmed by the calculated COHP shown in Figure 1c. Figure 1d,e shows the Cu-d and Se-p orbital components of the upper valence band. We can see that the two valence band extrema at the Γ and L points, namely, VBM and VB_1, are close in energy but with different orbital weights. The Cu-d orbital has almost the same contribution from the Γ point to the L point, while the Se-p orbital has a larger contribution at the Γ point than the L point. Therefore, it can be inferred that the p−d coupling strength at the Γ point is stronger than that at the L point. Thus, in order to tune the VBM and VB_1 closer in energy for higher valence band degeneracy, we could reduce the anti-bonding strength, which would shift the VBM downward more compared to VB_1. Such k-dependent orbital characters at the valence band edge of Cu_2Se offer the possibility for band modification.[45,46] For example, the anti-bonding strength at Γ and L points could be tuned by varying the atomic orbital energy difference between Cu-d and Se-p or Cu−Se bond length.[5]

https://doi.org/10.1021/acs.jpcc.2c08797
J. Phys. Chem. C XXXX, XXX, XXX−XXX

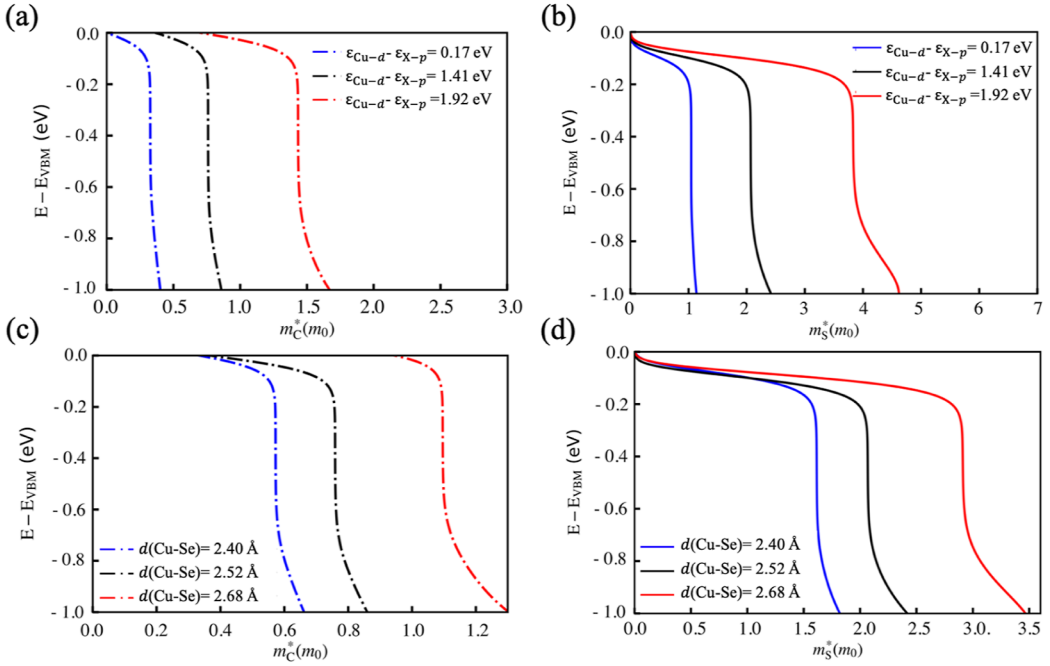

Figure 3. Energy dependence of conductivity effective mass, m_C^*, (a,c) and Seebeck effective mass, m_S^*, (b,d) at 800 K for p-type Cu_2X (X = S, Se, and Te).

To understand the sensitivity of the VBM and VB_1 values to the anti-bonding strength, with the primitive Cu_2Se, we have chemically shifted the relative position of the anion p atomic orbital by replacing Se with S and Te and also physically changed the bond length between Se and Cu, to adjust Cu-d and anion-p orbital coupling strength. Referring to Cu_2Se (black lines in Figure 2), the band structures of S- and Te-substituted variants with the fixed Cu−X (X = S, Se, and Te) bond length of 2.52 Å as same as Cu−Se bond length are presented in Figure 2a. It can be found that as the chalcogenide atom (X) changes from Te to Se to S, the VB_1 at the L point shifts upward closer to the VBM, and when the VBMs at the Γ point are aligned at the same energy level, the energy difference between VB_1 and VBM is 0.40, 0.69, and 1.09 eV for Cu_2S, Cu_2Se, and Cu_2Te, respectively. This can be attributed to the fact that atomic orbital energy differences between Cu-d and X-p increase with atomic number decreasing, which weakens the interatomic orbital interactions and reduces the valence band dispersion around the Fermi level, and thus, the energy offset between VBM and VB_1 becomes smaller. Figure 2b shows the band structures of Cu_2Se with different Cu−Se bond lengths, d(Cu−Se). Larger d(Cu−Se) decreases the energy separation between the VBM and VB_1 and leads to a better degeneracy and an increased DOS near the Fermi level. It is worth mentioning that bond length modulation has been achieved in experiments, for example, doping or substrate modulation.[47−49] In the work of Naatz et al., effective modulation of the Cu−O bond length by adding Fe to the CuO nanoparticles was achieved.[48] Moreover, Wang et al. induced large compressive thermal strain in the as-grown WS_2 by quartz with a large thermal expansion coefficient.[47] The orbital energy difference can be controlled by doping with different types of anions and cations.

To confirm the band structure, the total DOS of Cu_2X near the Fermi level with different p−d orbital energy differences and bond lengths are shown in Figure 2c,d with the zero energy level representing the VBMs. It is well known that a rapid change of the DOS near the VBM is a good indicator of large Seebeck coefficient. As shown in Figure 2c,d, the total DOS, which has a large slope stemming from the convergence of valence bands, can be obtained with a large energy split between Cu-d and X-p ($\varepsilon_{Cu\text{-}d}-\varepsilon_{X\text{-}p}$) orbitals or with a large bond length between Cu and Se (d(Cu−Se)). Figure 2e shows the influence of changing the anti-bonding strength on band convergence through changing the Cu-d and X-p orbital energy difference. It can be seen that while both VBM and VB_1 energy levels decrease with increasing the p−d orbital energy difference, the energy value of the VBM decreases much faster than VB_1, leading to the band convergence. A larger p−d orbital energy difference indicates a weaker anti-bonding strength as reflected by a smaller −ICOHP value. The bond length dependence of VBM and VB_1 energy levels shows similar trends in Figure 2f. A decrease in VBM, VB_1, VBM-VB_1, and the corresponding −ICOHP values all occur when the bond length is increased. This indicates that increasing $\varepsilon_{Cu\text{-}d}-\varepsilon_{X\text{-}p}$ or d(Cu−Se) to weaken the p−d anti-bonding strength is indeed helpful for converging valence bands for Cu_2Se.

The features of the electronic structures suggest that a weak anti-bonding interaction is preferable for Cu_2Se to achieve a high band degeneracy. To rationalize the interplay between the electronic structure and transport properties, the calculation of the Seebeck effective mass m_S^* and conductivity effective mass m_C^* is important to understand the thermoelectric performance, which are generally dependent on the features of the band structure around the Fermi level. As shown in Figure 3, both the effective masses m_S^* and m_C^* at 800 K increase with the increase of $\varepsilon_{Cu\text{-}d}-\varepsilon_{X\text{-}p}$ or d(Cu−Se), which is in line with the change of the valence band curvature. The enlarged m_S^* indicates an increase of the Seebeck coefficient; however, the larger m_C^* at the same time could lead to a poorer carrier mobility.

Thermoelectric properties of Cu_2X with different p−d hybridization strengths at 800 K were calculated using the

https://doi.org/10.1021/acs.jpcc.2c08797
J. Phys. Chem. C XXXX, XXX, XXX−XXX

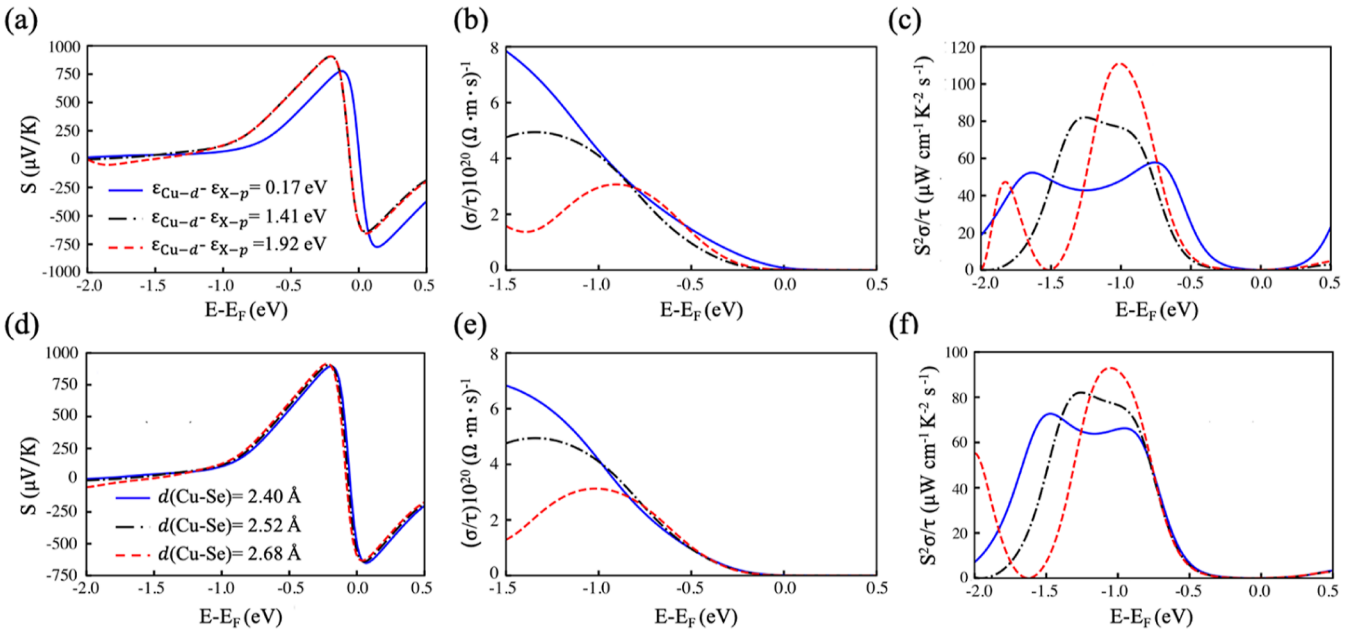

Figure 4. Calculated Seebeck coefficient S (a,d), electrical conductivity with respect to relaxation time σ/τ (b,e), and power factor with respect to relaxation time $S^2\sigma/\tau$ (c,f) at 800 K as a function of energy for Cu_2X (X = S, Se, and Te). The curves in (a−c) correspond to various atomic p−d orbital energy differences and various bond lengths in (d−f).

semiclassical Boltzmann transport equation that was implemented in BoltzTraP. Under rigid band approximation, the Fermi level can be tuned through doping (p-type or n-type), while the fundamental band structure is not changed. As illustrated in Figure 4a,d, increasing $\varepsilon_{Cu\text{-}d}-\varepsilon_{X\text{-}p}$ or d(Cu−Se) causes the Seebeck coefficient to increase as the Fermi level moves into the valence band (p-type doping), indicating that a weak p−d hybridization strength is more favorable to obtain a large S. Such phenomena are consistent with the calculated results of the Seebeck effective mass given in Figure 3b,d, since S shows a proportional relation with m_S^*. As can be seen in Figure 4b,e, in contrast to S, increasing $\varepsilon_{Cu\text{-}d}-\varepsilon_{X\text{-}p}$ or d(Cu−Se) causes a low σ/τ, as the anti-bonding Cu−Se becomes less hybridized, leading to electrical conductivity reduction. Combining S and σ/τ, the power factor ($S^2\sigma/\tau$) with respect to chemical potential is displayed in Figure 4c,f. $S^2\sigma/\tau$ shows an increasing tendency with the increase of $\varepsilon_{Cu\text{-}d}-\varepsilon_{X\text{-}p}$ or d(Cu−Se). Therefore, tuning the p−d hybridization through band engineering in the Cu site is possible to tune the TE performance.

Based on the above discussions, a high band degeneracy could be achieved in Cu_2Se by decreasing the p−d anti-bonding strength. In experiments, doping will be the most feasible way to adjust the anti-bonding strength and hence to finely tune a material's electronic structure. Decreasing the anti-bonding interaction between Cu-d and Se-p by choosing the dopants which can cause a larger on-site energy difference between cation-d and anion-p orbitals will lead to the convergence of the VBM and VB_1.

According to the calculated atomic energy levels of the Cu and Se atoms in Table 1, the Cu-3d orbital is 1.41 eV higher than the Se-4p orbital. Since the valence band edge is composed of the p−d anti-bonding state, modifying the on-site energy of the higher energy atomic orbital, corresponding to the Cu-3d orbital here, has a large impact on the anti-bonding state.[50] Hence, the introduction of the extrinsic dopant with a higher d orbital energy than Cu is likely to weaken the p−d interaction and converge the VBM and VB_1. In Table 1, we summarize some potential doping elements for achieving band convergence, according to their atomic energy levels. And, we select two elements M (M = Fe and Mn in Table 1) with a larger energy differences between M-d and Se-p, 2.05 and 2.12 eV for Fe and Mn, respectively. The larger the energy difference between Se-p and M-d, the lower is the anti-bonding strength, causing the convergence of the VBM and VB_1. With an appropriate doping concentration of Fe/Mn in Cu_2Se, the number of effective hole pockets is likely to be enlarged.

Table 1. Relevant Atomic Energy Levels of p and d Orbitals of Different Atoms

element	valence state	p orbital energy (eV)	d orbital energy (eV)
S	$3s^23p^4$	−6.80	
Se	$4s^24p^4$	−6.29	
Te	$5s^25p^4$	−5.59	
Cu	$3d^{10}4s^1$		−4.88
Fe	$3d^64s^2$		−4.24
Mn	$3d^54s^2$		−4.17

In addition to doping foreign atoms, introducing vacancies can also play a role in band structure modification.[30] In Cu_2Se, the introduced Cu vacancy (V_{Cu}) can be considered as a foreign dopant with d orbital energy of infinity, which does not make any contribution to the anti-bonding states near the valence band edge since there is no hybridization between V_{Cu} and the Se atom. Hence, introducing V_{Cu} is also possible to weaken the anti-bonding strength and improve the band degeneracy.

It is found that $V_{Cu}/Fe_{Cu}/Mn_{Cu}$ all could be applied to the band structure engineering of Cu_2Se. In this work, when introducing V_{Cu} in Cu_2Se, two Cu vacancy are considered in a $2 \times 2 \times 2$ supercell of Cu_2Se, and thus, its formula is $Cu_{14}Se_8$, corresponding to a hole concentration with a magnitude of 10^{21} cm^{-3}, which is in line with the experimental data of the high hole concentration in Cu_2Se. And, when alloying with Fe/

https://doi.org/10.1021/acs.jpcc.2c08797
J. Phys. Chem. C XXXX, XXX, XXX−XXX

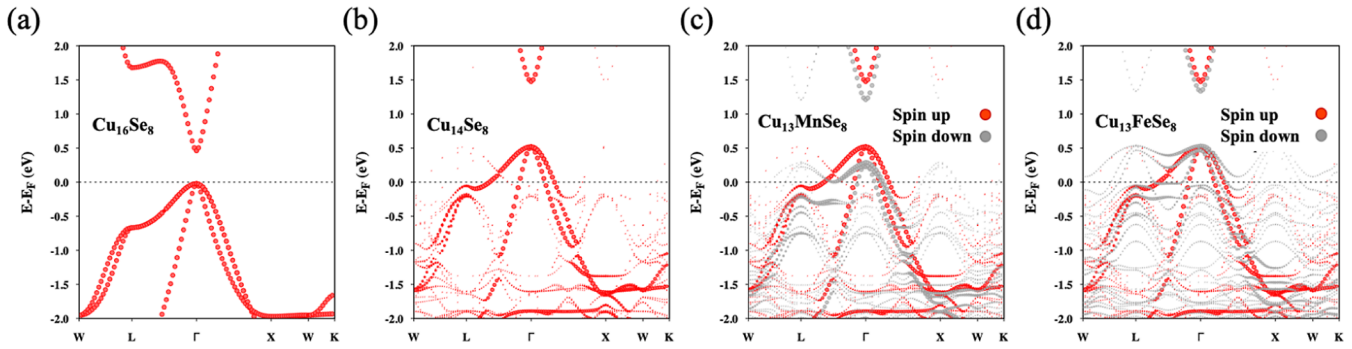

Figure 5. Effective band structures for (a) $Cu_{16}Se_8$, (b) $Cu_{14}Se_8$, (c) $Cu_{13}MnSe_8$, and (d) $Cu_{13}FeSe_8$.

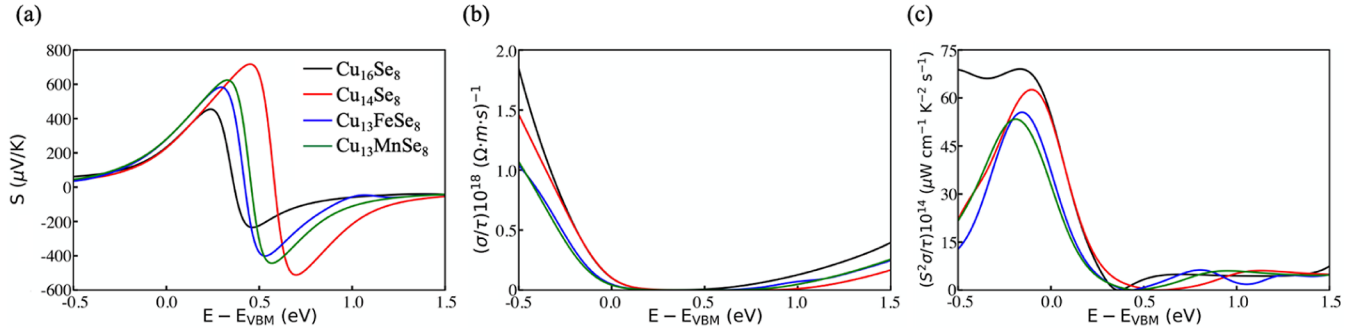

Figure 6. Calculated (a) Seebeck coefficient (S), (b) electrical conductivity with respect to relaxation time (σ/τ), and (c) power factor with respect to relaxation time ($S^2\sigma/\tau$) at 800 K as a function of energy for $Cu_{16}Se_8$, $Cu_{14}Se_8$, $Cu_{13}MnSe_8$, and $Cu_{13}FeSe_8$.

Mn in Cu_2Se, the transition metal dopants have been usually explored as multivalent species (+2, +3, +4, etc.),[51] while Cu has a valence state of +1. If one high-valence-state atom substitutes one Cu atom in the supercell, this will contribute extra valence electrons to the system and the system may adapt itself to extra charge by the creation of mid-gap states.[52,53] Given the unknown valence states of the dopants (Fe and Mn), different amounts of copper vacancies are introduced for investigating the correct ground-state electronic structures of M-doped Cu_2Se. Since the V_{Cu} and M pairs could have several different possible configurations, the one with the lowest energy has been our focus in the following discussion, and the corresponding configurations are displayed in the Supporting Information.

Figure 5 shows the comparison of the calculated band structures of $Cu_{16}Se_8$, $Cu_{14}Se_8$, $Cu_{13}MnSe_8$, and $Cu_{13}FeSe_8$. Because the calculations were conducted on supercell structures, the Brillouin zone size was reduced, leading to the folding of the bands. To compare these band structures to that of undoped Cu_2Se, the band structures of supercells were unfolded. As shown in Figure 5a,b, when introducing Cu vacancies into Cu_2Se, the band gap is enlarged from 0.50 to 0.90 eV and the energy separation of the two valence band maxima VBM and VB_1 is decreased from 0.65 to 0.60 eV. So, introducing V_{Cu} in Cu_2Se could slightly alter the electronic structure. For $Cu_{13}MnSe_8$ and $Cu_{13}FeSe_8$, as shown in Figure 5c,d, it can be found that the energy differences between the VBM and VB_1 become obviously smaller compared to the pristine compound $Cu_{16}Se_8$, presenting preferable band convergence because of the higher valley degeneracy at VB_1 than that at the VBM (8 vs 3). The greater contribution of valence bands with high degeneracy is expected to result in an enhancement of the Seebeck coefficient when the chemical potential is located around the valence band edge.

Based on the band structure results, the electronic transport properties can be obtained by utilizing the Boltzmann transport theory. Figure 6 shows the electronic transport properties of $Cu_{16}Se_8$, $Cu_{14}Se_8$, $Cu_{13}MnSe_8$, and $Cu_{13}FeSe_8$ as a function of Fermi energy at 800 K. As can be seen in Figure 6a, the defective Cu_2Se ($Cu_{14}Se_8$, $Cu_{13}MnSe_8$, and $Cu_{13}FeSe_8$) exhibits a higher Seebeck coefficient than perfect Cu_2Se ($Cu_{16}Se_8$). The increase of S can be explained by the changes of the Seebeck effective mass under the weakened p−d hybridization strength. On the other hand, the normalized electrical conductivity of Fe- and Mn-doped Cu_2Se is much lower than that of the pristine system. Hence, combining S and σ/τ, the normalized power factor ($S^2\sigma/\tau$) of Cu_2Se is higher than that of the Fe- and Mn-doped systems. This demonstrates that the introduction of Cu vacancies or Fe/Mn dopants into Cu_2Se has a detrimental effect on the electrical transport properties, which can be ascribed to the increased hole effective mass and band gap, leading to an obviously decreased electrical conductivity. It is noteworthy that the originally proposed band convergence strategy is considered to lead to high power factor; however, the intervalley scattering of carriers stemming from the converged bands is entirely overlooked and may impair the carrier mobility and electrical conductivity, leading to the band convergence ineffective in some thermoelectric systems, where more comprehensive band structure engineering to balance the carrier mobility and band degeneracy will be needed.

CONCLUSIONS

In conclusion, the thermoelectric properties of Cu_2Se are systematically studied by using the electronic structure calculations. The band structure calculations using the mBJ + U method reproduce the semiconducting behavior of Cu_2Se. It is found that the valence band edge of Cu_2Se is formed by the

https://doi.org/10.1021/acs.jpcc.2c08797
J. Phys. Chem. C XXXX, XXX, XXX−XXX

anti-bonding states of Cu-d and Se-p orbitals. The valence band morphology is determined by the p−d anti-bonding strength. Weakening the p−d anti-bonding strength through increasing the bond length between Cu and Se or increasing the atomic orbital energy difference between Cu-d and anion-p can decrease the energy offset between two valence band maxima at Γ and *L* points, respectively, and thus, it contributes to an improved band degeneracy. To tune the valence band toward a higher band degeneracy, the foreign dopants of Fe and Mn with a higher d atomic orbital energy level than Cu are introduced to soften the p−d anti-bonding strength. Simply introducing Cu vacancies can also reduce the p−d anti-bonding states near the valence band edge. The Seebeck coefficients for Fe/Mn-doped Cu_2Se and Cu_2Se with Cu vacancies are larger than those of the pristine compound; however, the lower conductivity for defects containing Cu_2Se resulting from the lower carrier mobility is the constraint for enhancement of power factor. The inter-valley scattering would counterbalance the benefit from the band convergence in Cu_2Se, which hence needs careful consideration in such multi-band systems. Our work not only suggests that Cu_2Se has great potential for further improvement as high-temperature thermoelectric materials but also provides general design rules to increase the band degeneracy through effective extrinsic doping for other thermoelectric materials.

■ ASSOCIATED CONTENT

Supporting Information

The Supporting Information is available free of charge at https://pubs.acs.org/doi/10.1021/acs.jpcc.2c08797.

Energy convergence test of the *k*-points, lattice parameters of intrinsic and defective Cu_2Se, selection of *U* for transition metal, selection of the calculation method for the band structure, comparison of the thermoelectric performances with and without fixed lattice vectors, and selection of doping configurations (PDF)

■ AUTHOR INFORMATION

Corresponding Author

Hong Zhu − *University of Michigan−Shanghai Jiao Tong University Joint Institute, Shanghai Jiao Tong University, Shanghai 200240, China;* orcid.org/0000-0001-7919-5661; Email: hong.zhu@sjtu.edu.cn

Authors

Xiaomeng Cai − *University of Michigan−Shanghai Jiao Tong University Joint Institute, Shanghai Jiao Tong University, Shanghai 200240, China*

Huirong Jing − *University of Michigan−Shanghai Jiao Tong University Joint Institute, Shanghai Jiao Tong University, Shanghai 200240, China*

Hexige Wuliji − *School of Materials Science and Engineering, Shanghai Jiao Tong University, Shanghai 200240, China*

Complete contact information is available at: https://pubs.acs.org/10.1021/acs.jpcc.2c08797

Author Contributions

§X.C. and H.J. contributed equally to this work and should be considered co-first authors.

Notes

The authors declare no competing financial interest.

■ ACKNOWLEDGMENTS

This work was supported by the National Natural Science Foundation of China (52072240) and the Materials Genome Initiative Center at Shanghai Jiao Tong University. All simulations were carried out with computational resources from the Shanghai Jiao Tong University High Performance Computing Center.

■ REFERENCES

(1) Acharyya, P.; Roychowdhury, S.; Samanta, M.; Biswas, K. Ultralow Thermal Conductivity, Enhanced Mechanical Stability, and High Thermoelectric Performance in $(GeTe)_{1-2x}(SnSe)_x(SnS)_x$. *J. Am. Chem. Soc.* **2020**, *142*, 20502−20508.

(2) Roychowdhury, S.; Ghosh, T.; Arora, R.; Waghmare, U. V.; Biswas, K. Stabilizing n-Type Cubic GeSe by Entropy-Driven Alloying of AgBiSe 2 : Ultralow Thermal Conductivity and Promising Thermoelectric Performance. *Angew. Chem.* **2018**, *130*, 15387−15391.

(3) Puneet, P.; Podila, R.; Karakaya, M.; Zhu, S.; He, J.; Tritt, T. M.; Dresselhaus, M. S.; Rao, A. M. Preferential Scattering by Interfacial Charged Defects for Enhanced Thermoelectric Performance in Few-layered N-type Bi_2Te_3. *Sci. Rep.* **2013**, *3*, 3212.

(4) Girard, S. N.; He, J.; Li, C.; Moses, S.; Wang, G.; Uher, C.; Dravid, V. P.; Kanatzidis, M. G. In Situ Nanostructure Generation and Evolution within a Bulk Thermoelectric Material to Reduce Lattice Thermal Conductivity. *Nano Lett.* **2010**, *10*, 2825−2831.

(5) Zhu, H.; Sun, W.; Armiento, R.; Lazic, P.; Ceder, G. Band Structure Engineering through Orbital Interaction for Enhanced Thermoelectric Power Factor. *Appl. Phys. Lett.* **2014**, *104*, 082107.

(6) Zeier, W. G.; Zhu, H.; Gibbs, M.; Tremel, G.; Snyder, W.; Jeffrey Snyder, G. Band Convergence in the Non-cubic Chalcopyrite Compounds Cu_2MGeSe_4. *J. Mater. Chem. C* **2014**, *2*, 10189−10194.

(7) Pei, Y.; Tan, G.; Feng, D.; Zheng, L.; Tan, Q.; Xie, X.; Gong, S.; Chen, Y.; Li, J.-F.; He, J.; Kanatzidis, M. G.; Zhao, L.-D. Integrating Band Structure Engineering with All-Scale Hierarchical Structuring for High Thermoelectric Performance in PbTe System. *Adv. Energy Mater.* **2017**, *7*, 1601450.

(8) Moshwan, R.; Liu, W.-D.; Shi, X.-L.; Wang, Y.-P.; Zou, J.; Chen, Z.-G. Realizing High Thermoelectric Properties of SnTe via Synergistic Band Engineering and Structure Engineering. *Nano Energy* **2019**, *65*, 104056.

(9) Gibbs, Z. M.; Ricci, F.; Li, G.; Zhu, H.; Persson, K.; Ceder, G.; Hautier, G.; Jain, A.; Snyder, G. J. Effective Mass and Fermi Surface Complexity Factor from Ab Initio Band Structure Calculations. *npj Comput. Mater.* **2017**, *3*, 8.

(10) Li, W.; Chen, Z.; Lin, S.; Chang, Y.; Ge, B.; Chen, Y.; Pei, Y. Band and Scattering Tuning for High Performance Thermoelectric $Sn_{1-x}Mn_xTe$ alloys. *J. Materiomics* **2015**, *1*, 307−315.

(11) Bhat, D. K.; Shenoy, U. S. Enhanced Thermoelectric Performance of Bulk Tin Telluride: Synergistic Effect of Calcium and Indium Co-Doping. *Mater. Today Phys.* **2018**, *4*, 12−18.

(12) Mukherjee, M.; Yumnam, G.; Singh, A. K. High Thermoelectric Figure of Merit via Tunable Valley Convergence Coupled Low Thermal Conductivity in $A^{II}B^{IV}C_2^{V}$ Chalcopyrites. *J. Phys. Chem. C* **2018**, *122*, 29150−29157.

(13) Pei, Y.; LaLonde, A. D.; Heinz, N. A.; Shi, X.; Iwanaga, S.; Wang, H.; Chen, L.; Snyder, G. J. Stabilizing the Optimal Carrier Concentration for High Thermoelectric Efficiency. *Adv. Mater.* **2011**, *23*, 5674−5678.

(14) Pei, Y.; Wang, H.; Gibbs, Z. M.; LaLonde, A. D.; Snyder, G. J. Thermopower Enhancement in $Pb_{1-x}Mn_xTe$ Alloys and its Effect on Thermoelectric Efficiency. *NPG Asia Mater.* **2012**, *4*, No. e28.

(15) Pei, Y.; LaLonde, A. D.; Heinz, N. A.; Snyder, G. J. High Thermoelectric Figure of Merit in PbTe Alloys Demonstrated in PbTe-CdTe. *Adv. Energy Mater.* **2012**, *2*, 670−675.

(16) Liu, W.; Tan, X.; Yin, K.; Liu, H.; Tang, X.; Shi, J.; Zhang, Q.; Uher, C. Convergence of Conduction Bands as a Means of Enhancing

Thermoelectric Performance of n-Type $Mg_2Si_{1-x}Sn_x$ Solid Solutions. *Phys. Rev. Lett.* **2012**, *108*, 166601.
(17) Zhao, K.; Liu, K.; Yue, Z.; Wang, Y.; Song, Q.; Li, J.; Guan, M.; Xu, Q.; Qiu, P.; Zhu, H.; Chen, L.; Shi, X. Are Cu_2Te-Based Compounds Excellent Thermoelectric Materials? *Adv. Mater.* **2019**, *31*, 1903480.
(18) Liu, H.; Shi, X.; Xu, F.; Zhang, L.; Zhang, W.; Chen, L.; Li, Q.; Uher, C.; Day, T.; Snyder, G. J. Copper Ion Liquid-like Thermoelectrics. *Nat. Mater.* **2012**, *11*, 422−425.
(19) Zhang, Z.; Zhao, K.; Wei, T.-R.; Qiu, P.; Chen, L.; Shi, X. Cu_2Se-Based Liquid-like Thermoelectric Materials: Looking Back and Stepping Forward. *Energy Environ. Sci.* **2020**, *13*, 3307−3329.
(20) Gahtori, B.; Bathula, S.; Tyagi, K.; Jayasimhadri, M.; Srivastava, A. K.; Singh, S.; Budhani, R. C.; Dhar, A. Giant Enhancement in Thermoelectric Performance of Copper Selenide by Incorporation of Different Nanoscale Dimensional Defect Features. *Nano Energy* **2015**, *13*, 36−46.
(21) Zhang, Y.; Wang, Y.; Xi, L.; Qiu, R.; Shi, X.; Zhang, P.; Zhang, W. Electronic Structure of Antifluorite Cu_2X (X = S, Se, Te) within the Modified Becke-Johnson Potential Plus an On-site Coulomb U. *J. Chem. Phys.* **2014**, *140*, 074702.
(22) Råsander, M.; Bergqvist, L.; Delin, A. Density Functional Theory Study of the Electronic Structure of Fluorite Cu_2Se. *J. Phys.: Condens. Matter* **2013**, *25*, 125503.
(23) Tyagi, K.; Gahtori, B.; Bathula, S.; Auluck, S.; Dhar, A. Band Structure and Transport Studies of Copper Selenide: An Efficient Thermoelectric Material. *Appl. Phys. Lett.* **2014**, *105*, 173905.
(24) Hu, Q.; Zhu, Z.; Zhang, Y.; Li, X.-J.; Song, H.; Zhang, Y. Remarkably High Thermoelectric Performance of $Cu_{2-x}Li_xSe$ bulks with nanopores. *J. Mater. Chem. A* **2018**, *6*, 23417−23424.
(25) Bhardwaj, R.; Bhattacharya, A.; Tyagi, K.; Gahtori, B.; Chauhan, N. S.; Vishwakarma, A.; Johari, K. K.; Bathula, S.; Auluck, S.; Dhar, A. Enhancement in Thermoelectric Performance of Single Step Synthesized Mg Doped Cu_2Se: An Experimental and Theoretical Study. *Intermetallics* **2019**, *112*, 106541.
(26) Liao, W.-W.; Yang, L.; Chen, J.; Zhou, D.-L.; Qu, X.; Zheng, K.; Han, G.; Zhou, J.-B.; Hong, M.; Chen, Z.-G. Realizing Bi-doped α-Cu_2Se as a Promising Near-Room-Temperature Thermoelectric Material. *Chem. Eng. J.* **2019**, *371*, 593−599.
(27) Peng, P.; Gong, Z. N.; Liu, F. S.; Huang, M. J.; Ao, W. Q.; Li, Y.; Li, J. Q. Structure and Thermoelectric Performance of β-Cu_2Se Doped with Fe, Ni, Mn, In, Zn or Sm. *Intermetallics* **2016**, *75*, 72−78.
(28) Yao, M.; Liu, W.; Chen, X.; Ren, Z.; Wilson, S.; Ren, Z.; Opeil, C. Low Temperature Thermoelectric Properties of P-Type Copper Selenide with Ni, Te and Zn Dopants. *J. Alloys Compd.* **2017**, *699*, 718−721.
(29) Mukherjee, S.; Parasuraman, R.; Umarji, A. M.; Rogl, G.; Rogl, P.; Chattopadhyay, K. Effect of Fe Alloying on the Thermoelectric Performance of Cu_2Te. *J. Alloys Compd.* **2020**, *817*, 152729.
(30) Tan, X.; Shao, H.; He, J.; Liu, G.; Xu, J.; Jiang, J.; Jiang, H. Band Engineering and Improved Thermoelectric Performance in M-Doped SnTe (M = Mg, Mn, Cd, and Hg). *Phys. Chem. Chem. Phys.* **2016**, *18*, 7141−7147.
(31) Park, J.; Dylla, M.; Xia, Y.; Wood, M.; Snyder, G. J.; Jain, A. When Band Convergence is not Beneficial for Thermoelectrics. *Nat. Commun.* **2021**, *12*, 3425.
(32) Xiong, F.; Tan, H. B.; Xia, C.; Chen, Y. Strain and Doping in Two-Dimensional SnTe Nanosheets: Implications for Thermoelectric Conversion. *ACS Appl. Nano Mater.* **2020**, *3*, 114−119.
(33) Xia, C.; Cui, J.; Chen, Y. Effect of Group-3 Elements Doping on Promotion of In-plane Seebeck Coefficient of n-Type Mg_3Sb_2. *J. Materiomics* **2020**, *6*, 274−279.
(34) Kresse, G.; Furthmüller, J. Efficient Iterative Schemes for Ab Initio Total-Energy Calculations Using a Plane-Wave Basis Set. *Phys. Rev. B: Condens. Matter Mater. Phys.* **1996**, *54*, 11169−11186.
(35) Kohn, W.; Sham, L. J. Self-Consistent Equations Including Exchange and Correlation Effects. *Phys. Rev.* **1965**, *140*, A1133−A1138.
(36) Blöchl, P. E. Projector Augmented-Wave Method. *Phys. Rev. B: Condens. Matter Mater. Phys.* **1994**, *50*, 17953−17979.
(37) Perdew, J. P.; Burke, K.; Ernzerhof, M. Generalized Gradient Approximation Made Simple. *Phys. Rev. Lett.* **1996**, *77*, 3865−3868.
(38) Tran, F.; Blaha, P. Accurate Band Gaps of Semiconductors and Insulators with a Semilocal Exchange-Correlation Potential. *Phys. Rev. Lett.* **2009**, *102*, 226401.
(39) Deringer, V. L.; Tchougréeff, A. L.; Dronskowski, R. Crystal Orbital Hamilton Population (COHP) Analysis as Projected from Plane-Wave Basis Sets. *J. Phys. Chem. A* **2011**, *115*, 5461−5466.
(40) Dronskowski, R.; Bloechl, P. E. Crystal Orbital Hamilton Populations (COHP): Energy-Resolved Visualization of Chemical Bonding in Solids Based on Density-Functional Calculations. *J. Phys. Chem.* **1993**, *97*, 8617−8624.
(41) Nelson, R.; Ertural, C.; George, J.; Deringer, V. L.; Hautier, G.; Dronskowski, R. LOBSTER : Local Orbital Projections, Atomic Charges, and Chemical-Bonding Analysis from Projector-Augmented-Wave-based Density-Functional Theory. *J. Comput. Chem.* **2020**, *41*, 1931−1940.
(42) Wang, V.; Xu, N.; Liu, J.; Tang, G.; Geng, W. VASPKIT: a User-Friendly Interface Facilitating High-Throughput Computing and Analysis Using VASP Code. *Comput. Phys. Commun.* **2021**, *267*, 108033.
(43) Madsen, G. K. H.; Singh, D. J. BoltzTraP. A Code for Calculating Band-Structure Dependent Quantities. *Comput. Phys. Commun.* **2006**, *175*, 67−71.
(44) Sorokin, G. P.; Papshev, Y. M.; Oush, P. T. Photoconductivity of Cu_2S, Cu_2Se and Cu_2Te. *Sov. Phys. Solid State* **1966**, *7*, 1810.
(45) Tan, X.; Wang, L.; Shao, H.; Yue, S.; Xu, J.; Liu, G.; Jiang, H.; Jiang, J. Improving Thermoelectric Performance of α-MgAgSb by Theoretical Band Engineering Design. *Adv. Energy Mater.* **2017**, *7*, 1700076.
(46) Feng, Z.; Zhang, X.; Wang, Y.; Zhang, J.; Jia, T.; Cao, B.; Zhang, Y. Thermoelectric Optimization of $AgBiSe_2$ by Defect Engineering for Room-Temperature applications. *Phys. Rev. B* **2019**, *99*, 155203.
(47) Wang, J.; Luo, Y.; Cai, X.; Shi, R.; Wang, W.; Li, T.; Wu, Z.; Zhang, O.; Peng, A.; Amini, C.; Tang, K.; Liu, N.; Wang, C.; Cheng, C. Multiple Regulation over Growth Direction, Band Structure, and Dimension of Monolayer WS_2 by a Quartz Substrate. *Chem. Mater.* **2020**, *32*, 2508−2517.
(48) Naatz, H.; Lin, S.; Li, W.; Jiang, Z.; Ji, C. H.; Chang, J.; Köser, J.; Thöming, T.; Xia, A. E.; Nel, L.; et al. Safe-by-Design CuO Nanoparticles via Fe-Doping, Cu-O Bond Length Variation, and Biological Assessment in Cells and Zebrafish Embryos. *ACS Nano* **2017**, *11*, 501−515.
(49) Jeong, M. H.; Sanger, A.; Kang, S. B.; Jung, Y. S.; Oh, I. S.; Yoo, J. W.; Kim, K. J.; Choi, K. J. Increasing the Thermoelectric Power Factor of Solvent-Treated PEDOT:PSS Thin Films on PDMS by Stretching. *J. Mater. Chem. A* **2018**, *6*, 15621−15629.
(50) Brod, M. K.; Anand, S.; Snyder, G. J. The Importance of Avoided Crossings in Understanding High Valley Degeneracy in Half-Heusler Thermoelectric Semiconductors. *Adv. Electron. Mater.* **2022**, *8*, 2101367.
(51) Telesca, D.; Nie, Y.; Budnick, J. I.; Wells, B. O.; Sinkovic, B. Impact of Valence States on the Superconductivity of Iron Telluride and Iron Selenide Films with Incorporated Oxygen. *Phys. Rev. B: Condens. Matter Mater. Phys.* **2012**, *85*, 214517.
(52) Hoang, K.; Mahanti, S. D. Electronic Structure of Ga-, In-, and Tl-Doped PbTe: a Supercell Study of the Impurity Bands. *Phys. Rev. B: Condens. Matter Mater. Phys.* **2008**, *78*, 085111.
(53) Yu, W.; Zhu, Z.; Niu, C.-Y.; Li, C.; Cho, J.-H.; Jia, Y. Anomalous Doping Effect in Black Phosphorene Using First-principles Calculations. *Phys. Chem. Chem. Phys.* **2015**, *17*, 16351−16358.

https://doi.org/10.1021/acs.jpcc.2c08797
J. Phys. Chem. C XXXX, XXX, XXX−XXX